Progress In Electromagnetics Research M, Vol. 90, 127–135, 2020

Optimization of Gimbal Parameters to Improve the Boresight Error Performance of Airborne Radomes

Yash S. Zanwar, A. P. Aparna, and Hrishikesh S. Sonalikar*

Abstract—This paper presents the effect of gimbal geometry parameters on the electromagnetic performance of streamlined radome for airborne applications. The work demonstrates that the gimbal position significantly affects the boresight error performance. The optimization of gimbal position is performed, and the resultant boresight error is limited to 1.5 mrad while keeping the insertion loss below 0.25 dB over the entire antenna scan angle range. The analysis of the antenna-radome system is carried out using the 3D ray tracing method. This work shows that the gimbal geometry parameters provide additional degree of freedom for improving radome performance parameters and can be applied to both the gimbal mounted and electronically scanning antennas enclosed by streamlined radomes.

1. INTRODUCTION

A radome is a structure that protects an antenna from its operating environment [1]. Presence of radome can cause degradation in antenna performance due to the introduction of undesirable effects such as boresight error and Transmission Loss [2]. In airborne applications, radome needs to satisfy stringent structural, electromagnetic, and temperature requirements [3]. As a result, radome needs to be carefully designed after choosing appropriate materials [4].

The design of airborne radomes remains an active topic of research due to challenges posed by stringent and often contradictory requirements in airborne environment. A new hybrid cone-ogive radome with variable thickness was proposed in [5] for improvement over a conventional constant thickness radome. The radome with inhomogeneous wall having exponential variation of dielectric constant was proposed in [6] in order to obtain better power transmission characteristics. A graded porous radome wall made of Silicon Nitride was proposed for high velocity applications in [7]. A 7-layer constant thickness radome design with gradual variation of dielectric constant in different layers was proposed in [8] to obtain a performance comparable to variable thickness radome by improving the impedance matching. A design of a constant thickness monolithic radome was presented with temperature dependent analysis for hypersonic applications in [9]. A dual band radome with sandwich wall construction was proposed in [10]. Xu et al. proposed new radome design methods based on particle swarm optimization [11], better thickness profiling [12, 17], and reflector shaping [13] to obtain improved radome electromagnetic (EM) performance [14–16]. In all these works, a typical antenna radome system was analyzed using the geometrical optics based 3D ray tracing method in conjunction with aperture integration. The focus of the radome design strategy was usually to optimize the radome wall parameters such as thickness, number of layers, and dielectric constant in order to improve the power transmission and boresight error characteristics of the radome.

The antenna enclosed by a nose-cone airborne radome is usually mounted on a gimbal to facilitate scanning in elevation and azimuth directions. For newer generation radars based on phased array antennas, the scanning is performed electronically by modifying the feeds to individual antenna elements.

Received 21 January 2020, Accepted 5 March 2020, Scheduled 11 March 2020
* Corresponding author: Hrishikesh Shashikant Sonalikar (hrishikeshs@goa.bits-pilani.ac.in).
The authors are with the Department of Electrical and Electronics Engineering, Goa Campus, BITS Pilani, India.

In most of the recently reported works, the enclosed antenna was assumed situated at a fixed position on the radome axis, and offsets corresponding to elevation and azimuth gimbals were assumed to be zero. The effect of changing the antenna position or the gimbal offsets is not studied, and the possibility of using these parameters to improve the performance of antenna-radome system is not explored. The position of the antenna and effect of gimbal offsets can affect the radome performance in airborne applications as the view of the streamlined radome as seen from the antenna will change with these parameters.

Therefore, the objective of this paper is to analyze the effect of the gimbal offsets and gimbal position (antenna position) on the radome performance parameters like Bore Sight Error (BSE) and Power Transmission (PT). An attempt is also made to optimize the gimbal position to improve the performance of the radome. 3D ray tracing method [1] developed in house is used for this purpose. It will be shown that the BSE characteristics of the radome are significantly improved by optimizing the gimbal position. The radome performance is demonstrated by numerically computing PT, BSE, aperture phase distribution and antenna patterns.

Section 2 presents the antenna-radome configuration used in this work. Section 3 presents the outline of 3D ray tracing method with the focus on coordinate transformation to incorporate gimbal rotations. Section 4 presents results and discussion. Finally, Section 5 presents the concluding remarks.

2. ANTENNA RADOME CONFIGURATION

Figure 1 shows the geometry of the tangent ogive radome considered in this work. The radome has a length of 1 m and a base diameter of 0.5 m. The radome has a monolithic wall made of a material having the dielectric constant of 5.7617 and loss tangent of 0.00261. The array antenna enclosed inside the radome has an aperture having a diameter of 0.2 m. The antenna array operates at the frequency of 10 GHz. The aperture has a rectangular grid of 100 source points (antenna elements) placed half wavelength apart. The antenna is mounted on a gimbal. The gimbal can rotate in both elevation plane and azimuth plane. Depending on the first plane of rotation, the gimbal can be considered as either elevation-over-azimuth (EL/AZ) type or azimuth-over-elevation (AZ/EL) type. In this work, the EL/AZ type of gimbal is considered. The center of the gimbal is located at a distance X_g from the base of the radome. The incident electric fields from the source points are assumed vertically polarized. Optimum power transmission through the radome is ensured by optimizing the radome wall thickness at 6.91 mm for perpendicular polarization and at maximum angle of incidence.

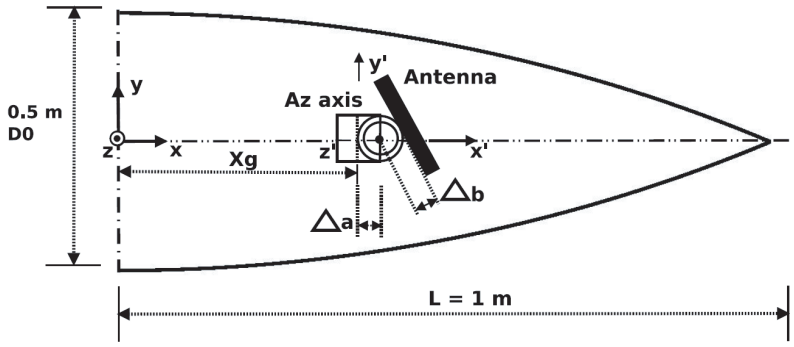

Figure 1. Geometry for radome-enclosed antenna mounted on EL/AZ type of gimbal.

3. 3D RAY TRACING METHOD

In this work, the 3D ray tracing method is used for the analysis of a radome enclosed antenna system. This method is suitable for the relatively fast analysis of electrically large structures such as airborne radomes on personal computers. Ray tracing is preferred if dimensions of the antenna are around five wavelengths [10]. 3D ray tracing performs the coordinate transformation of source points, computes

point of intersection of rays and radome wall, as well as angle of incidence and transmission coefficient of each ray. It subsequently finds the antenna sum pattern which is then used for predicting the performance parameters of radomes. As the focus of this paper is on optimization of gimbal geometry parameters, the transformation of coordinates from the antenna coordinate system to the radome coordinate system by incorporating gimbal rotations will be discussed in more detail.

In this paper, the antenna is assumed to be mounted on elevation-over-azimuth (EL/AZ) type of gimbal. Fig. 1 shows the antenna coordinate system (x', y', z') with the origin situated at the gimbal position and the radome coordinate system (x, y, z) with the origin situated at the center of the radome base. In EL/AZ type of gimbal, first the antenna is rotated around the elevation axis z' in anticlockwise direction through an angle EL measured from x'-z' plane. The elevation offset is Δb. Then the antenna is rotated around the azimuth axis y' in clockwise direction through angle AZ measured from x'-y' plane. The azimuth offset is Δa. To transform the coordinates of a given point from the antenna coordinate system to the radome coordinate system, it is necessary to derive rotation matrices by incorporating the gimbal offsets.

Suppose that the coordinates of a given point in the antenna coordinate system are (x_a, y_a, z_a). Then the coordinates after the anticlockwise rotation around elevation axis z' through elevation angle EL are given by

$$\begin{aligned} x_1 &= (x_a + \Delta b)\cos EL - y_a \sin EL \\ y_1 &= (x_a + \Delta b)\sin EL + y_a \cos EL \\ z_1 &= z_a. \end{aligned} \tag{1}$$

In matrix form, this equation can be represented as,

$$\begin{bmatrix} x_1 \\ y_1 \\ z_1 \end{bmatrix} = \begin{bmatrix} \cos EL & -\sin EL & 0 \\ \sin EL & \cos EL & 0 \\ 0 & 0 & 1 \end{bmatrix} \begin{bmatrix} x_a + \Delta b \\ y_a \\ z_a \end{bmatrix}. \tag{2}$$

Similarly, the coordinates after the clockwise rotation around the azimuth axis y' through the azimuth angle AZ are given by

$$\begin{aligned} x_2 &= (x_1 + \Delta a)\cos AZ - z_1 \sin AZ \\ y_2 &= y_1 \\ z_2 &= (x_1 + \Delta a)\sin AZ + z_1 \cos AZ. \end{aligned} \tag{3}$$

In the matrix form, this equation can be represented as,

$$\begin{bmatrix} x_2 \\ y_2 \\ z_2 \end{bmatrix} = \begin{bmatrix} \cos AZ & 0 & -\sin EL \\ 0 & 1 & 0 \\ \sin AZ & 0 & \cos AZ \end{bmatrix} \begin{bmatrix} x_1 + \Delta a \\ y_1 \\ z_1 \end{bmatrix}. \tag{4}$$

Finally, adding the gimbal position X_g, the coordinates in the radome coordinate system are given by

$$\begin{bmatrix} x_3 \\ y_3 \\ z_3 \end{bmatrix} = \begin{bmatrix} x_2 \\ y_2 \\ z_2 \end{bmatrix} + \begin{bmatrix} X_g \\ 0 \\ 0 \end{bmatrix}. \tag{5}$$

Equations (2), (4), and (5) can be combined into a single matrix equation for computer implementation. In a similar way, the coordinate transformation matrix for azimuth-over-elevation (AZ/EL) gimbal can be obtained.

After the coordinate transformation, the rays are constructed from each source point; the points of intersection of rays with radome wall are computed; the angles of incidence are determined; and the transmission coefficient T of each ray for a given radome wall configuration is obtained using equivalent transmission line model with locally planar radome wall. Finally, the antenna sum pattern is calculated as [1],

$$S = \frac{\sum_{i=1}^{M} F_a e^{-j\sin\theta(y_i\cos\phi + z_i\sin\phi)} T_i}{\sum_{i=1}^{M} F_a}. \tag{6}$$

where F_a is the aperture field distribution.

Radome performance parameters such as PT and BSE can be calculated from antenna sum pattern peak as

$$\text{PT} = 20\log_{10}(|S_{peak}|) \tag{7}$$

$$\text{BSE} = \text{angle}(|S_{peak}|) \tag{8}$$

where S_{peak} is the antenna sum pattern peak, and 'angle' means the angular location of sum pattern peak.

4. RESULTS AND DISCUSSION

In this section, the effect of elevation and azimuth offsets of gimbal as well as gimbal position on radome EM performance parameters is presented. Optimization of the gimbal position is performed to improve the radome performance. The results for the EL/AZ type of gimbal are presented.

In order to study the effect of gimbal geometry parameters on the radome performance, first the elevation and azimuth offsets are considered. Fig. 2 shows the variation of radome BSE with respect to antenna scan angle in the elevation plane for different values of the elevation offset Δb. The values of azimuth offset Δa and gimbal position X_g are set to 0 mm and 0.3 m, respectively. The minimum and maximum values of Δb are 0 mm and 20 mm, respectively. It can be observed that the BSE of the radome shows a marginal variation in the antenna scan angle range of 0 to 40°. The variation in BSE becomes very small for higher antenna scan angles. Therefore, it can be concluded that the changes in Δb do not significantly affect the BSE performance of the radome. Similar observations are obtained in the azimuth plane. Additionally, the power transmission performance of the radome is observed to be insensitive to the changes in Δb. Computation of the BSE and PT for different values of Δa results in a similar observation and hence not shown. As a result, it can be concluded that the changes in elevation and azimuth gimbal offsets have marginal effect on BSE performance and negligible effect on PT performance of the radome.

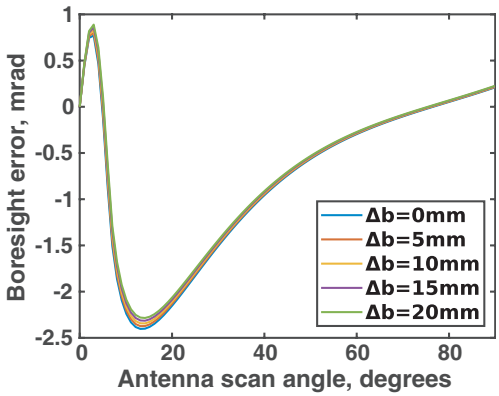

Figure 2. Variation in BSE with respect to antenna scan angle in elevation plane for different Δb values.

Next, the effect of gimbal position X_g on the radome performance is analyzed. For this analysis, the minimum value of X_g is set to 10 cm to accommodate the antenna aperture at the maximum antenna scan angle of 90°. The maximum value of X_g is set to 78 cm at which the diameter of the antenna aperture becomes equal to that of the radome. This analysis is done with both elevation and azimuth offsets set to 0 mm. The antenna is scanned in both elevation and azimuth planes from 0° to 90°.

Figures 3(a) and 3(b) show the variation in BSE with antenna scan angle in the elevation and azimuth planes, respectively, for 10 different values of gimbal position X_g. For both the elevation and azimuth places, it can be observed that the BSE performance of the radome changes from negative values to positive values as X_g is increased. It is also found that BSE remains within the acceptable

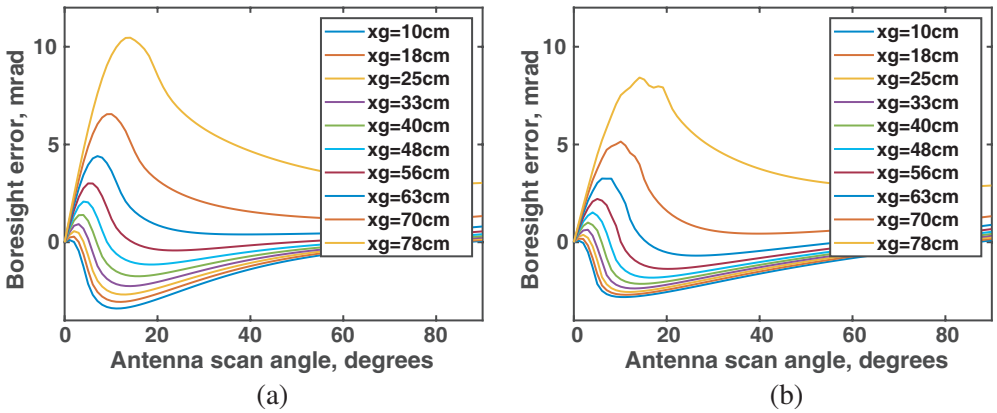

Figure 3. Variation in BSE with antenna scan angle for different values of X_g, in (a) elevation plane and (b) azimuth plane.

range of ± 2 mrad for X_g values between 40 cm and 48 cm. The optimum value of X_g at which the best possible BSE performance is achieved in both the planes is 44 cm.

Figures 4(a) and 4(b) show the variation in power transmission performance of the radome in the elevation and azimuth planes, respectively, as X_g is varied from the minimum to the maximum value. In the elevation plane, it can be observed that the antenna scan angle at which PT achieves minimum values shifts towards the lower values as X_g is increased, but the minimum value of PT does not change significantly. In the azimuth plane, the PT characteristics are improved with the increase in X_g. It can be noted that the overall PT performance remains satisfactory as the insertion loss is less than 0.3 dB for all values of X_g.

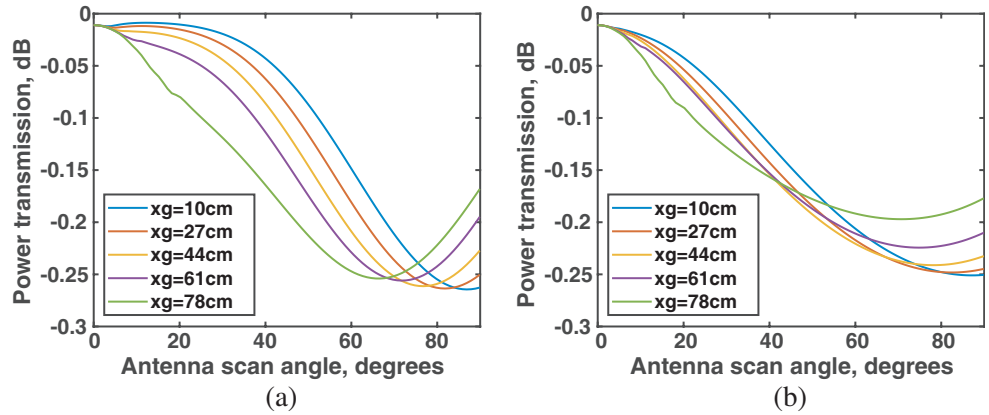

Figure 4. Variation in PT with antenna scan angle for different values of X_g in (a) elevation plane and (b) azimuth plane.

In order to obtain a physical insight about how the BSE performance of the radome is affected by the gimbal position X_g, the antenna aperture phase distribution and the sum pattern are computed at different gimbal positions and chosen values of antenna scan angle in both the planes. The four gimbal positions chosen for this purpose include the minimum value of 10 cm, the maximum value of 78 cm, the optimum value of 44 cm, and an additional value of 30 cm. The aperture phase distribution is calculated at these offsets for two scan angles, 5° and 20°, respectively.

Figures 5(a) and 5(b) show the aperture phase distribution at an antenna scan angle of 5° in the elevation and azimuth planes, respectively. The corresponding antenna sum pattern in the elevation plane is shown in Fig. 6. It can be observed that variation in X_g significantly affects the phase distribution. Also, the phase distribution at $X_g = 78$ cm is drastically asymmetric compared to that at

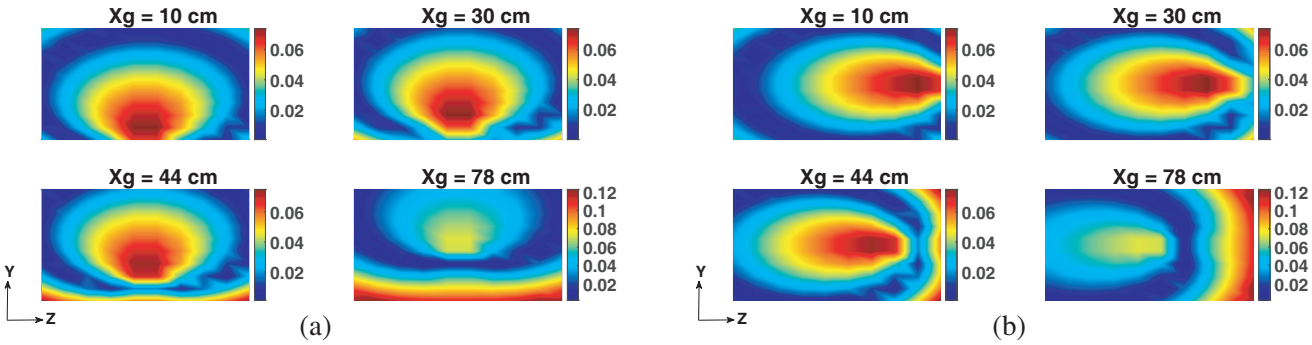

Figure 5. Aperture phase distribution at the antenna scan angle of 5° for different X_g values in (a) the elevation plane and (b) the azimuth plane.

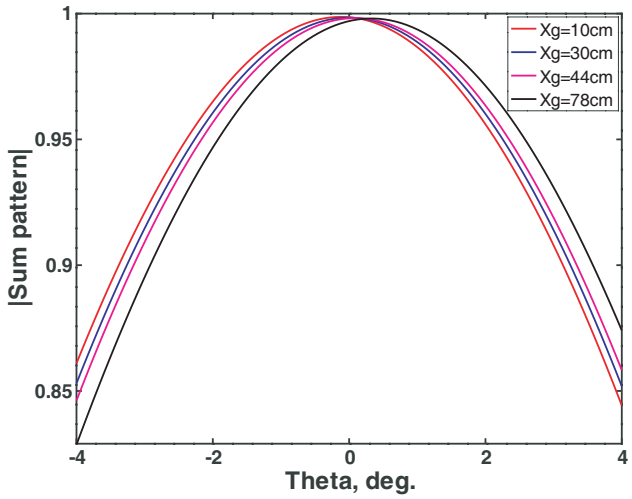

Figure 6. Antenna sum patterns at the scan angle of 5° in elevation plane for different X_g values.

lower values of X_g. As a result, the antenna sum pattern peak can be seen significantly shifted from the antenna axis at $X_g = 78$ cm, resulting in large BSE. As X_g is increased from 10 cm to 44 cm, a slight change of phase can be observed at the edges of the aperture. These changes produce slight shifts of antenna peak as seen in Fig. 6. The shifted peaks of the antenna sum pattern produce BSE.

Figures 7(a) and 7(b) show the aperture phase distribution at an antenna scan angle of 20° in the elevation and azimuth planes, respectively. The corresponding antenna sum pattern in the elevation plane is shown in Fig. 8. At this scan angle also, a relatively lower difference between the minimum and maximum phases is observed for X_g values of 10, 30, and 44 cm. This results in a slight shift of antenna sum pattern peak and produces a relatively lower values of BSE. A drastically changed phase distribution is observed at $X_g = 78$ cm, which in turn causes a larger shift in antenna sum pattern peak and higher BSE.

In order to take advantage of the improvement in BSE due to proper selection of gimbal position, the radome wall thickness is optimized again at $X_g = 44$ cm. Table 1 shows the optimized radome wall thicknesses for the initial and the optimized antenna gimbal positions. The table also lists the maximum angle of incidence at which the wall thickness optimization is performed and the corresponding antenna scan angle. A small decrease in the optimum radome wall thickness can be noted at a new gimbal position. The radome EM performance parameters of these two radomes are now compared.

Figures 9(a) and 9(b) show the variations in PT and BSE with antenna scan angle, respectively for two radomes optimized at $X_g = 30$ cm and $X_g = 44$ cm. It can be observed that the radome with $X_g = 30$ cm has slightly better PT up to high antenna scan angles. On the other hand, BSE performance

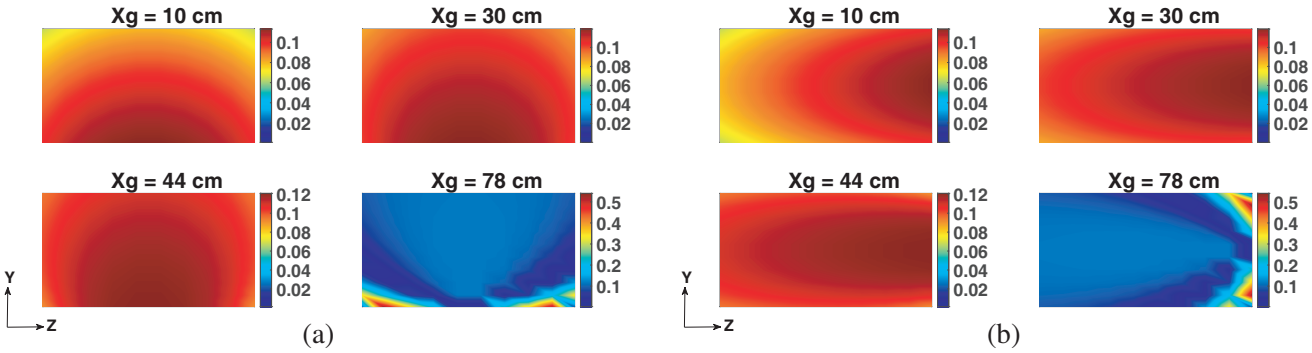

Figure 7. Aperture phase distribution at the antenna scan angle of 20° for different X_g values in (a) the elevation plane and (b) the azimuth plane.

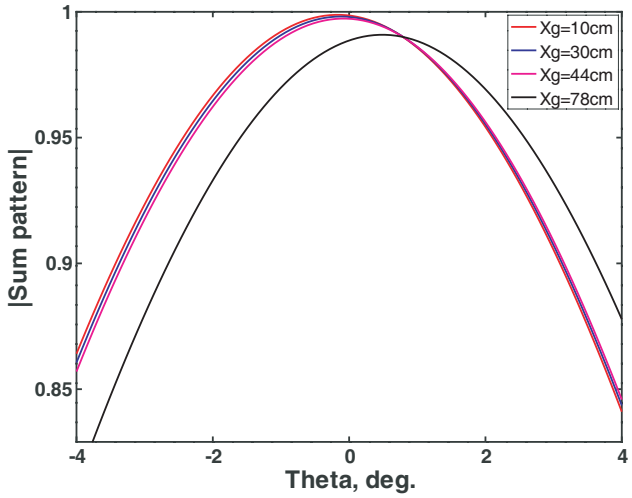

Figure 8. Antenna sum patterns at the scan angle of 20° in elevation plane for different X_g values.

Table 1. Optimization of radome wall thickness at different gimbal positions X_g.

X_g (m)	Antenna Scan Angle (Deg.)	Maximum angle of incidence (Deg.)	Wall thickness (mm)
0.30	3	67.714	6.9109
0.44	4	69.303	6.9079

Table 2. A comparison of the proposed work with the published literature.

Reference	X_g (m)	L (m)	Optimized Parameters	Number of Layers	Max. Magnitude of BSE (mrad)	Radome Geometry	Type of Radome
[8]	0.3	1	Thickness	7	2.5	Tangent ogive	CTR
[9]	0.08	0.4	Thickness	6	1.9	Tangent ogive	CTR
[10]	0.3	1	Thickness	3	3.8	Tangent ogive	CTR
[11]	0.3	1	Thickness	1	0.5445	Cone ogive	VTR
[18]	0.411	1.4	Thickness	7	2.3	Tangent ogive	CTR
Proposed work	0.44	1	Thickness and X_g	1	1.5	Tangent ogive	CTR

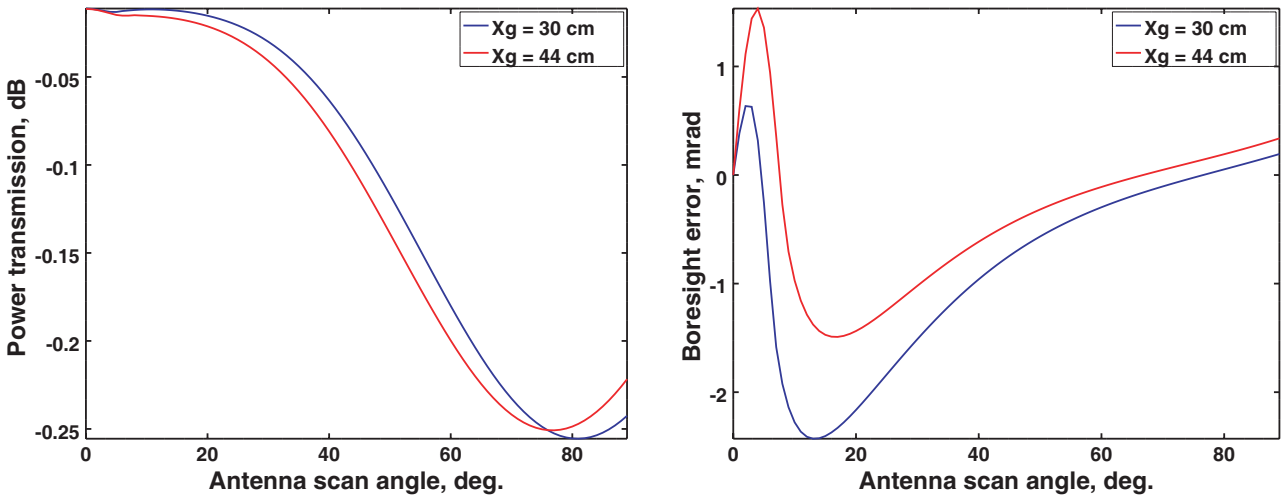

Figure 9. Power transmission and boresight error performance of the radome with initial and optimized values of X_g.

of radome with $X_g = 44\,\text{cm}$ is significantly improved.

Table 2 shows the comparison of the radome design proposed in this work with the airborne radome designs presented in the recent literature. It is clear that the BSE performance of the proposed radome is superior to all the constant thickness radome designs. The results presented here are also comparable to those obtained using particle swarm optimization in [11].

5. CONCLUSION

This paper presents an analysis of the effects of antenna gimbal offsets and gimbal position on radome performance. The analysis is performed by varying the gimbal offsets as well as position and predicting the BSE and PT performances of radome as a function of antenna scan angles in both elevation and azimuth planes. It is observed that the azimuth and elevation offsets have negligible effect on radome performance. On the other hand, the gimbal position affects both BSE and PT significantly and shows that these findings are also applicable to the electronically scanning antennas. Consequently, the BSE performance of the radome is significantly improved by limiting the BSE values within the range of $\pm 1.5\,\text{mrad}$. The mechanism of effect of gimbal parameters on radome BSE performance is demonstrated by computing aperture phase distribution and antenna sum patterns. This work suggests that the optimization of gimbal parameters provides additional degree of freedom to improve the radome performance. The experimental verification of the presented findings will be taken and presented in the future communications.

REFERENCES

1. Kozakoff, D. J., *Analysis of Radome-Enclosed Antennas*, 2nd Edition, Artech House, 2010.
2. Shavit, R., *Radome Electromagnetic Theory and Design*, Wiley Online Library, 2018.
3. Cady, W. M., M. B. Karelitz, and L. A. Turner, *Radar Scanners and Radomes*, Vol. 26, McGraw-Hill Book Company, 1948.
4. Crone, G. A. E., A. W. Rudge, and G. N. Taylor, "Design and performance of airborne radomes: A review," *IEE Proc.*, Vol. 128, 451–464, 1981.
5. Nair, R. U. and R. M. Jha, "Electromagnetic performance analysis of a novel monolithic radome for airborne applications," *IEEE Transactions on Antennas and Propagation*, Vol. 57, 3664–3668, 2009.

6. Nair, R. U., S. Shashidhara, and R. Jha, "Novel inhomogeneous planar layer radome design for airborne applications," *IEEE Antennas and Wireless Propagation Letters*, Vol. 11, 854–856, 2012.
7. Chen, F., Q. Shen, and L. Zhang, "Electromagnetic optimal design and preparation of broadband ceramic radome material with graded porous structure," *Progress In Electromagnetics Research*, Vol. 105, 445–461, 2010.
8. Nair, R., M. Suprava, and R. Jha, "Graded dielectric inhomogeneous streamlined radome for airborne applications," *Electronics Letters*, Vol. 51, No. 11, 862–863, 2015.
9. Nair, R. U., S. Vandhana, and R. M. Jha, "Temperature-dependant electromagnetic performance predictions of a hypersonic streamlined radome", *Progress In Electromagnetics Research*, Vol. 154, 65–78, 2015.
10. Zhou, L., Y. Pei, and D. Fang, "Dual-band A-sandwich radome design for airborne applications," *IEEE Antennas and Wireless Propagation Letters*, Vol. 15, 218–221, 2015.
11. Xu, W., B. Y. Duan, P. Li, N. Hu, and Y. Qiu, "Multiobjective particle swarm optimization of boresight error and transmission loss for airborne radomes", *IEEE Transactions on Antennas and Propagation*, Vol. 62, No. 11, 5880–5885, 2014.
12. Xu, W., B. Duan, P. Li, and Y. Qiu, "A new efficient thickness profile design method for streamlined airborne radomes," *IEEE Transactions on Antennas and Propagation*, Vol. 65, No. 11, 6190–6195, 2017.
13. Xu, W., B. Duan, P. Li, Y. Zong, and Y. Qiu, "Novel compensation method for electromagnetic performance of dielectric radome based on reflector shaping," *IET Microwaves, Antennas & Propagation*, Vol. 9, No. 2, 125–132, 2014.
14. Xu, W., B. Duan, P. Li, and Y. Qiu, "Study on the electromagnetic performance of inhomogeneous radomes for airborne applications. Part I: Characteristics of phase distortion and boresight error," *IEEE Transactions on Antennas and Propagation*, Vol. 65, No. 6, 3162–3174, 2017.
15. Xu, W., B. Duan, P. Li, and Y. Qiu, "Study on the electromagnetic performance of inhomogeneous radomes for airborne applications. Part II: The overall comparison with variable thickness radomes," *IEEE Transactions on Antennas and Propagation*, Vol. 65, No. 6, 3175–3183, 2017.
16. Xu, W., P. Li, and Y. Qiu, "Electromagnetic performance analysis of inhomogeneous airborne radomes for circular polarization applications," *IEEE Antennas and Wireless Propagation Letters*, Vol. 18, No. 1, 74–78, 2018.
17. Xu, W., P. Li, and Y. Qiu, "Efficient variable thickness radome design with insertion phase delay correction," *International Journal of Antennas and Propagation*, No. 9150361, 1–12, 2019.
18. Yazeen, P. M., C. Vinisha, S. Vandana, M. Suprava, and R. U. Nair, "Electromagnetic performance analysis of graded dielectric inhomogeneous streamlined airborne radome," *IEEE Transactions on Antennas and Propagation*, Vol. 65, No. 5, 2718–2723, 2017.